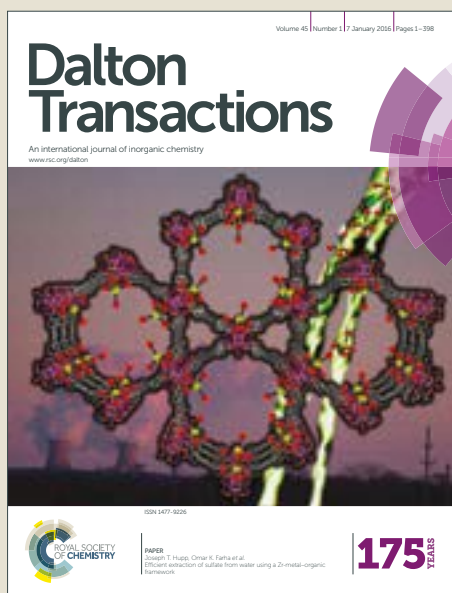


# Dalton Transactions

Accepted Manuscript



This article can be cited before page numbers have been issued, to do this please use: A. D'Annibale, R. Panetta, O. Tarquini, M. Colapietro, S. Quaranta, A. Cassetta, L. Barba, G. Chita and A. Latini, *Dalton Trans.*, 2019, DOI: 10.1039/C9DT00690G.



This is an Accepted Manuscript, which has been through the Royal Society of Chemistry peer review process and has been accepted for publication.

Accepted Manuscripts are published online shortly after acceptance, before technical editing, formatting and proof reading. Using this free service, authors can make their results available to the community, in citable form, before we publish the edited article. We will replace this Accepted Manuscript with the edited and formatted Advance Article as soon as it is available.

You can find more information about Accepted Manuscripts in the [author guidelines](#).

Please note that technical editing may introduce minor changes to the text and/or graphics, which may alter content. The journal's standard [Terms & Conditions](#) and the ethical guidelines, outlined in our [author and reviewer resource centre](#), still apply. In no event shall the Royal Society of Chemistry be held responsible for any errors or omissions in this Accepted Manuscript or any consequences arising from the use of any information it contains.

# Synthesis, Physico-Chemical Characterization and Structure of the Elusive Hydroxylammonium Lead Iodide Perovskite $\text{NH}_3\text{OHPbI}_3$

Andrea D'Annibale<sup>1</sup>, Riccardo Panetta<sup>1</sup>, Ombretta Tarquini<sup>2</sup>, Marcello Colapietro<sup>2</sup>, Simone Quaranta<sup>3</sup>, Alberto Cassetta<sup>4</sup>, Luisa Barba<sup>4</sup>, Giuseppe Chita<sup>4</sup>, Alessandro Latini<sup>1\*</sup>

<sup>1</sup> Dipartimento di Chimica, Università degli Studi di Roma "La Sapienza", Piazzale Aldo Moro 5, 00185 Roma, Italy

<sup>2</sup> Consiglio Nazionale delle Ricerche - Istituto di Cristallografia, Via Salaria km 29,300, 00015 Monterotondo Scalo, Roma, Italy

<sup>3</sup> Dipartimento di Ingegneria dell'Informazione, Elettronica e Telecomunicazioni, Università degli Studi di Roma "La Sapienza", Via Eudossiana, 18, 00184 Roma, Italy

<sup>4</sup> Consiglio Nazionale delle Ricerche - Istituto di Cristallografia, Sede Secondaria di Trieste, Area Science Park – Basovizza, Strada Statale 14, km 163.5, 34149 Trieste, Italy

\*corresponding author. Email: [alessandro.latini@uniroma1.it](mailto:alessandro.latini@uniroma1.it)

**ABSTRACT:** The synthesis of hydroxylammonium lead iodide  $\text{NH}_3\text{OHPbI}_3$  was accomplished by means of the reaction between water solutions of HI and  $\text{NH}_2\text{OH}$  with  $\text{PbI}_2$  in sulfolane in conjunction with either crystallization by  $\text{CH}_2\text{Cl}_2$  vapor diffusion or sulfolane extraction with toluene. The appropriate choice of the solvent was found to be crucial in order to attain the desired material. The synthesized compound was extensively characterized by single crystal and powder X-ray diffraction, UV-Vis diffuse reflectance spectroscopy, FT-IR spectroscopy,  $^1\text{H-NMR}$  spectroscopy, TG-DTA-QMS EGA (Evolved Gas Analysis), ESI-MS, and CHNS analysis.  $\text{NH}_3\text{OHPbI}_3$  is an extremely reactive, deliquescent solid that easily oxidizes in air releasing iodine. Furthermore, it is the first reported perovskite to melt (m.p. around 80 °C) before decomposing exothermally at 103 °C. Such a chemical behavior, together with its optical absorption properties (i.e. yellow-colored perovskite), renders this material totally unsuitable for photovoltaic applications. The deliquescence of the material is to be ascribed to the strong hydrophilicity of hydroxylammonium ion. On the other hand, the relatively high Brønsted acidity of hydroxylammonium ( $\text{pK}_a=5.97$ ) compared to other ammonium cations, promotes the reduction of atmospheric oxygen to water and the  $\text{NH}_3\text{OHPbI}_3$  oxidation. The crystal structure, determined by single crystal X-ray diffraction with synchrotron radiation, is orthorhombic, but differs from the prototypal perovskite structure. Indeed it comprises infinite chains of face-sharing  $\text{PbI}_6$  octahedra along the *c*-axis direction with hydroxylammonium cations positioned

between the columns, forming layers on the *ac* plane. The solvent intercalates easily between the layers. The crystal structure is apparently anomalous considering that the expected Goldschmidt's tolerance factor for the system (0.909) lies in the range of a stable prototypal perovskite structure. Therefore, the strong hydrogen bond forming tendency of hydroxylamine is likely to account for the apparent structural anomaly.

View Article Online  
DOI: 10.1039/C9DT00090G

## 1. Introduction

Methylammonium lead iodide ( $\text{CH}_3\text{NH}_3\text{PbI}_3$ ) has been emerging as one of the most promising photovoltaic materials. Thereby, an intense research activity has been promoted worldwide over the last ten years in order to maximize the performances of perovskite-based solar cells and improve their stability. Indeed,  $\text{CH}_3\text{NH}_3\text{PbI}_3$  has already proven to be susceptible to thermal and chemical degradation<sup>1</sup>. Among the countless (organo)ammonium cations forming  $\text{APbI}_3$  (A=ammonium cation) lead iodides, only a few possessing proper dimensions are able to form perovskitic structures. Conversely, too large or too small cations lead to the so-called “yellow” perovskites. Such compounds are characterized by crystal structures unrelated to the prototypal one and, consequently, do not show optical properties amenable to solar cells applications<sup>2</sup>. Hence, plenty of research, mostly predicated on the Goldschmidt’s tolerance factor rule, has been devoted to the synthesis of stable perovskitic structures for many ammonium cation/metal cation/anion combinations<sup>3</sup>. Since the hydroxylammonium ion possesses an estimated ionic radius almost identical to the methylammonium one, it is an attractive ammonium cation for perovskite systems based on the divalent lead (cation)/iodine (anion) pair<sup>3</sup>. Theoretical calculations<sup>4</sup> also suggest that  $\text{NH}_3\text{OHPbI}_3$  may exist in a stable perovskitic phase. Thus, hydroxylammonium lead iodide could possibly manifest optical and electronic properties similar to the  $\text{CH}_3\text{NH}_3\text{PbI}_3$  ones. Therefore, investigations on the synthesis and characterization of lead-iodine-ammonium perovskites relying on the  $\text{NH}_3\text{OH}^+$  cation are to be considered highly desirable.

A paper reporting the synthesis of hydrazinium lead iodides together with the unsuccessful synthesis of hydroxylammonium lead iodide has been recently published<sup>5</sup>. Needless to say, even  $\text{N}_2\text{H}_5^+$  has a calculated ionic radius nearly identical to that of methylammonium. Hence, hydrazinium lead iodides with two different stoichiometries (i.e.  $(\text{N}_2\text{H}_5)_{15}\text{Pb}_3\text{I}_{21}$  and  $\text{N}_2\text{H}_5\text{PbI}_3$ ) have been prepared. Although the latter compound matches the stoichiometric composition of a perovskite, neither of its two experimentally found polymorphs has turned out to own the correct structure. In fact, both polymorphs do not comply with the tolerance factor rule probably because of the substantial contribution to the lattice energy brought about by the hydrogen bond. Thus, the formation of crystal structures other than the perovskite prototype is most likely favored by the presence of hydrogen bonds. In addition, none of the authors’ attempts to synthesize the hydroxylammonium lead iodide by reacting hydroxylammonium iodide with lead iodide in 2-propanol and in dimethylformamide (DMF) has succeed. The ineffectiveness of their synthetic approaches stems from multiple causes. First,  $\text{PbI}_2$  is not soluble in 2-propanol. Second, hydroxylamine reacts with DMF producing dimethylamine and formohydroxamic acid. Indeed, amides (as other carboxylic and carbonyl compounds) are reactive towards hydroxylamine<sup>6,7</sup>. Nonetheless, a 2017 paper<sup>8</sup> reports the successful

synthesis of the  $\text{NH}_3\text{OHPbI}_2\text{Cl}$  mixed halide hydroxylammonium perovskite. However, the results presented are rather doubtful for various reasons. The most important issues are the reaction solvent used (DMF) and the questionable results concerning the thermogravimetric analysis, in which the exothermic decomposition of the hydroxylammonium moiety is not visible. Furthermore, the mass loss is not compatible with the claimed composition.

A simple approach to the synthesis of hydroxylammonium lead iodide, based on the method adopted by Poglitsch and Weber<sup>9</sup> for the preparation of methylammonium lead iodide, was initially used in the present research. Such a procedure had been already successfully employed by the authors for the synthesis of different perovskites<sup>10,11,12</sup>. Briefly, a 50% aqueous solution of hydroxylamine was added to a warm (50-60 °C) solution of lead (II) acetate in an excess of 57% aqueous HI. No precipitate formed also when a large excess of  $\text{NH}_2\text{OH}$  was added to the solution. Conversely, a yellow solid of very complex and still unidentified composition did precipitate by cooling the solution with an ice-water bath. Dissolution of this solid in DMF (1g of solid in 2 ml of solvent) and subsequent exposition of the solution to  $\text{CH}_2\text{Cl}_2$  vapor in a closed container resulted in the formation of two distinct solid phases. Specifically, a white, unstable powder and yellow crystals were collected at the bottom of the container. The former might probably be a mixture of lead formohydroxamate and other salts, while the latter was found out to be dimethylammonium lead iodide  $\text{NH}_2(\text{CH}_3)_2\text{PbI}_3$  by X-ray powder diffraction<sup>13</sup> and CHNS analysis. Such results verified the DMF decomposition by hydroxylamine. On the other hand, being the dimethylammonium lead iodide very soluble in DMF, only the white powder precipitation occurred when the  $\text{CH}_2\text{Cl}_2$  exposition step was skipped. After ruling out both the Poglitsch and Weber method and the use of DMF, a selection of one or more solvents suitable for a direct reaction between  $\text{NH}_3\text{OHI}$  and  $\text{PbI}_2$  (i.e. in order to avoid the production of interfering species) was undertaken. The appropriate solvent was to be chosen among the highly dipolar aprotic ones for ensuring dissolution of the ionic compounds formed during the reaction. Besides, other two requirements needed to be fulfilled by the solvent:

- being chemically inert with respect to hydroxylamine;
- showing little or no tendency to form thermally resistant adducts with  $\text{PbI}_2$ . Indeed, any heat treatment exceeding 100 °C would jeopardize the hydroxylamine chemical stability (i.e.  $\text{NH}_2\text{OH}$  decomposes at about 100 °C).

Such restrictions excluded all the common solvents such as the amides, gamma-butyrolactone, N-methylpyrrolidone (all these solvents are attacked by hydroxylamine), and dimethylsulfoxide, that forms stable, and therefore non-removable (i.e. for temperatures lower than 100°C) adducts with  $\text{PbI}_2$ <sup>14</sup>. The only stable and commercially available solvents satisfying the above requirements are either sulfolane or N-alkylated cyclic ureas like N,N'-dimethylpropyleneurea (DMPU) and 1,3-

dimethyl-2-imidazolidinone (DMI). Sulfolane and DMI were consequently picked out as solvents for the  $\text{NH}_3\text{OHPbI}_3$  synthesis. DMI was chosen because of its lower donor number<sup>15,16</sup> (27.7) compared to DMPU (33). Judging by DMF and DMSO donor numbers (27 and 29.8, respectively) and chemical structures, DMI was considered to be less prone to form stable adducts with  $\text{PbI}_2$  than DMPU. Pure  $\text{PbI}_2$  is insoluble in sulfolane (even hot) due to the low donor number of the solvent (14.8). Both sulfolane and DMI are highly polar (i.e. dipole moments equal to 4.69 and 4.09 debye, respectively), chemically and thermally very stable, and possess high values of the relative dielectric constant (43.4 and 37.6 respectively)<sup>17,18</sup>.

## 2. Experimental Section

**2.1 Materials preparation.** Lead (II) nitrate  $\text{Pb}(\text{NO}_3)_2$  (99%) was purchased from Alfa Aesar. Hydriodic acid HI 57% aqueous solution (<1.5% hypophosphorous acid as stabilizer), hydroxylamine  $\text{NH}_2\text{OH}$  (50% solution in water), 1,3-dimethyl-2-imidazolidinone ( $\geq 99.5\%$ , over molecular sieves) and sulfolane (99%) were purchased from Sigma Aldrich. Toluene (99.8%) was purchased from VWR. Absolute ethanol and dichloromethane (both  $\geq 99.9\%$ ) were purchased from Carlo Erba Reagents. The synthesis of  $\text{NH}_3\text{OHPbI}_3$  was performed in both sulfolane and DMI by reacting freshly prepared  $\text{NH}_3\text{OHI}$  with an equimolar amount of  $\text{PbI}_2$  powder. Lead iodide had been previously prepared by reacting aqueous lead nitrate with aqueous hydriodic acid. In a typical synthesis, 286  $\mu\text{l}$  of 57% aqueous HI and 133  $\mu\text{l}$  of 50% aqueous  $\text{NH}_2\text{OH}$  were added under stirring to 2 ml of absolute ethanol in a 50 ml two necked round bottom flask at room temperature and under nitrogen atmosphere. Immediately the solution became bright yellow, then colorless. After stirring for 2-3 minutes the ethanol was removed under vacuum at 55 °C until the liquid started turning from colorless to light yellow. Such a step was carried out in order to prevent  $\text{NH}_3\text{OHI}$  from decomposing evolving iodine. Then, nitrogen was let into the flask and 4 ml of solvent were introduced with flowing nitrogen under stirring, followed by the addition of 1 g of  $\text{PbI}_2$ . The suspension was stirred under nitrogen until  $\text{PbI}_2$  completely dissolved. The solution was filtered through a 0.45  $\mu\text{m}$  PTFE syringe filter in a new 12 ml glass vial. The vial was inserted in a 100 ml Pyrex bottle that had been half-filled with dichloromethane and closed in an argon atmosphere. The solution was let nucleate overnight and bright yellow crystals begun appearing the following morning. Crystals stemming from the synthesis in sulfolane were needle-shaped (i.e. acicular), while the ones obtained through the DMI route were polyhedral. Crystal formation and growth took about a week to complete. Then, the vial was removed from the bottle and the crystals were filtered. According to the results attained by CHNS and DTA-TG analyses the crystals for the DMI case turned out to be made of an adduct between DMI and  $\text{PbI}_2$ . Specifically, the C:H:N ratio and the thermal decomposition pattern (i.e. endothermal decomposition) agree perfectly with the DMI- $\text{PbI}_2$  adduct composition. In fact, the decomposition of the

hydroxylamine moiety is associated to an exothermal DTA signal. Hence, DMI was proved to be unsuitable for the hydroxylammonium lead iodide synthesis. Therefore, the results presented in the paper concern only the synthesis in sulfolane, which actually resulted into  $\text{NH}_3\text{OHPbI}_3$  crystals. Moreover,  $\text{NH}_3\text{OHPbI}_3$  powder could be collected from the solution by extracting the sulfolane with toluene. After the dissolution of  $\text{PbI}_2$  in the  $\text{NH}_3\text{OHI}$ /sulfolane solution, the liquid is transferred to a 100 ml glass centrifuge tube. Then, 50 ml of toluene are added, the mixture is stirred and then centrifuged at 2000 rpm for 2 minutes, the supernatant liquid was discarded and the whole process is repeated. After the second washing, a yellow solid forms and it is washed and centrifuged three times with 50 ml of clean toluene each time as above.

**2.2 Single crystal X-ray diffraction.** Single crystal X-ray diffraction measurements were performed at the XRD1 beamline of the Elettra synchrotron radiation facility (Trieste, Italy)<sup>19,20</sup>. Crystals were immersed in paraffin oil in order to avoid their reaction with air. A suitable crystal  $0.07 \times 0.05 \times 0.05$  mm<sup>3</sup> was selected with a loop and mounted on a goniometer head. A X-ray wavelength of 0.7 Å and a silicon diode array area detector (Pilatus 2 M; Dectris) were used for diffraction measurements. The crystal was kept at a steady  $T = 100$  K during data collection to prevent its degradation. Unit cell assignment, integration and data reduction were performed with the XDS program<sup>21</sup>. The structure was solved with the Superflip<sup>22</sup> structure solution software and by using Olex2 as the graphical interface<sup>23</sup>. The model was refined with version 2018/3 of ShelXL using least squares minimisation<sup>24</sup>. Sulfolane disorder was modeled in order to locate the hydroxylammonium ions. The electron density corresponding to their presence was located using PLATON/SQUEEZE<sup>25</sup>.

**2.3 Powder X-ray diffraction.** X-ray diffraction patterns were acquired using a Panalytical X'Pert Pro MPD diffractometer (Cu  $K\alpha$  radiation,  $\lambda=1.54184$  Å). The diffractometer is fitted with a X'Celerator RTMS detector. The angular resolution in  $2\theta$  is  $0.001^\circ$ ; 0.04 rad soller slit,  $1/4^\circ$  divergence slit, 15 mm mask on the incident beam path, 5.0 mm anti-scatter slit, Ni  $K\beta$  filter, 0.04 rad collimator on the diffracted beam path were used for the measurements. The scans were performed in the  $7.5\text{-}90^\circ$  in  $2\theta$  angular range. Rietveld refinement of the pattern of the powder sample was performed by means of the MAUD software package<sup>26</sup>.

**2.4 Thermogravimetry-Differential Thermal Analysis (TG-DTA)-Quadrupole Mass Spectrometry Evolved Gas Analysis (QMS-EGA).** TG-DTA analysis was performed with a Netzsch STA 409 PC Luxx thermal analyzer. The evolved gas analysis was performed by coupling the thermal analyzer with a Balzers-Pfeiffer QMG 421 quadrupole mass spectrometer ( $m/z$  range 0-128). The coupling was achieved by connecting the inlet of the mass spectrometer to the outlet of the TG-DTA apparatus through a stainless steel capillary heated at  $150$  °C to prevent moisture condensation. The measurements were performed in sintered alumina crucibles under flowing Ar

atmosphere (85 cm<sup>3</sup>/min @ STP, purity ≥ 99.9995%) with a scan rate of 10 K/min in the range RT-500 °C.

**2.5 UV-Vis spectroscopy.** Reflectance UV-Vis spectrum was acquired with a Shimadzu (Japan) UV2600 UV-Vis spectrophotometer equipped with a ISR-2600 Plus integrating sphere. BaSO<sub>4</sub> powder was the reflectance reference. The type of the band gap (i.e. direct or indirect, allowed or forbidden) was determined by comparing the absorption edge attained from the pseudoabsorbance spectrum with the values obtained with Tauc's plots<sup>27</sup> constructed for different exponents.

**2.6 FT-IR spectroscopy.** A Bruker Alpha spectrophotometer was used to acquire the FT-IR spectra in the 400-4000 cm<sup>-1</sup> wavenumber range (resolution 1 cm<sup>-1</sup>) in DRIFT mode on samples dispersed in dry KBr powder.

**2.7 ESI-MS.** A Finnigan-Mat LCQ mass spectrometer was used for the ESI-MS analysis of the powder sample. Since DMI is liquid at room temperature (while sulfolane melts at 27.5 °C) the reaction product was dissolved in DMI (1 mg/ml) in order to perform the analysis. Only positive ions were analyzed. The operating conditions were optimized for the analysis, i.e.: spray voltage 5.00 kV, capillary temperature 275 °C, capillary voltage 6 V, tube lens offset -5.00 V. The spray voltage value was chosen according to literature data<sup>28</sup>.

**2.8 CHN analysis.** The C, H, N and S contents of the single crystals sample was determined with a EA 1110 CHNS-O instrument.

**2.9. <sup>1</sup>H NMR.** <sup>1</sup>H NMR spectral analysis of the product synthesized in sulfolane was performed to verify the presence of the hydroxylammonium cation. The spectrum was acquired on a sample prepared dissolving single crystals of NH<sub>3</sub>OHPbI<sub>3</sub> in DMSO-d<sub>6</sub> using a 400 MHz Bruker Avance III spectrometer.

### 3. Results and Discussion.

**3.1 General considerations.** NH<sub>3</sub>OHPbI<sub>3</sub> as single crystals appears in the form of pale yellow needles, while when prepared as powder it is a bright yellow solid. Both forms of NH<sub>3</sub>OHPbI<sub>3</sub> are reactive materials, quickly darkening due to formation of elemental iodine by atmospheric oxygen oxidation favored by the relatively high acidity of the hydroxylammonium ion (pK<sub>a</sub>=5.97)<sup>29</sup>. The presence of free iodine after the exposure to air was confirmed by washing the darkened sample with hexane, which immediately became purple. It is also deliquescent as demonstrated by fig. 1, in which the freshly prepared powder is shown on the left and on the right the same sample is shown after 3 days at ambient conditions, appearing as a dark sludge. Thus, samples could be preserved for prolonged time only in sealed glass ampules under inert atmosphere. The reactivity and instability of the material impeded any kind of laser techniques (Raman, PL) investigation. In fact, even exposure of the sample to the lowest possible power density decomposed the material.

### 3.2 Structure determination.

View Article Online  
DOI: 10.1039/C9DT00690G

**Crystal Data.**  $C_6H_{20}I_3NO_3PbS$ ,  $M_r = 774.18$ , orthorhombic,  $Pm\bar{m}a$  (No. 51),  $a = 7.920(6)$  Å,  $b = 9.030(4)$  Å,  $c = 10.770(2)$  Å,  $\alpha = \beta = \gamma = 90^\circ$ ,  $V = 770.25(1)$  Å<sup>3</sup>,  $T = 100$  K,  $Z = 2$ ,  $Z' = 0.25$ ,  $\mu = 17.091$ , 6502 reflections measured, 1360 unique ( $R_{int} = 0.0392$ ) which were used in all calculations. The final  $wR_2$  was 0.1259 (all data) and  $R_1$  was 0.0394 ( $I > 2(I)$ ).

The structure of  $NH_3OHPbI_3$  is reported in fig. 2 and the data are summarized in table 1. The unit cell is orthorhombic (space group  $Pm\bar{m}a$ , no. 51) with lattice constants (at 100 K)  $a=7.920(6)$  Å,  $b=9.030(4)$  Å and  $c=10.770(2)$  Å, containing 2 formula units. The density is low (pycnometric:  $2.9\pm 0.5$  g cm<sup>-3</sup>, calculated:  $3.338$  g cm<sup>-3</sup>), due to the layered assembly of the hydroxylammonium-lead iodide moieties on the  $ac$  planes. The distance between the layers is  $\sim 4.7$  Å along the  $b$  axis. Lead and iodine atoms are arranged in infinite chains of face sharing octahedra along the  $a$  direction. As in other ammonium lead iodides the distances between the lead atom and the two iodine atoms of the asymmetric unit are different because of the effect of the lead  $6s^2$  lone pair<sup>12</sup>, so the  $PbI_6$  octahedra are distorted (bond lengths and angles are reported in the Supporting Information). Hydroxylammonium ions are positioned between the Pb-I chains on the  $ac$  plane. The structural motif of the hydroxylammonium ions is comprised of chains along the  $a$  direction (parallel to Pb-I chains) formed by 8 positions per unit cell in which the 2 hydroxylammonium ions are randomly distributed. The chain motif and its sinusoidal trend (fig. 3) are clearly indicative of strong and geometrically optimized interactions between the individual units.

Sulfolane molecules are able to be accommodated between the layers because of the hydrogen bonds formed with the hydroxylammonium ions. The maximum quantity of sulfolane molecules found in the single crystals (1 per formula unit  $NH_3OHPbI_3$ ), corresponds to a sulfolane content of about 16 wt. %. Nonetheless, sulfolane can be removed from the structure quite easily. Indeed, after multiple washings of the powder samples with toluene (which is unreactive towards  $NH_3OHPbI_3$  but functions as a solvent for sulfolane), the quantity of sulfolane decreased to about 10 wt. %, as demonstrated by thermal and CHNS analyses. Hence, a solvent with properties very close to those of sulfolane but more easily removable, such as piperylene sulfone<sup>30</sup> would probably allow to obtain pure  $NH_3OHPbI_3$ . Unfortunately, piperylene sulfone is not commercially available yet and, therefore, could not be tested.

Despite of evidence provided by recent and revised approaches, the  $NH_3OHPbI_3$  crystal structure did not correspond to the perovskite-type one expected from the tolerance factor calculations<sup>3</sup>. Using the available data, in fact,  $NH_3OHPbI_3$  showed a calculated tolerance factor of 0.909, nearly identical to that of  $CH_3NH_3PbI_3$  (0.912). Perovskite structures are expected for tolerance factors between 0.8 and 1. As mentioned in the introduction, also hydrazinium lead iodide (tolerance factor 0.912) does not

possess a perovskite structure although it fulfills the requirement on the tolerance factor. The authors reasonably assumed that the most probable reason is the tendency of hydrazinium ions to form hydrogen bonds. Provided that such explanation stands valid for the hydrazinium, it should be even more valid for the hydroxylammonium that contains the OH group. Hydroxylammonium tendency to form hydrogen bonds is already known for modifying the crystal structures of compound compared to its congeners<sup>31</sup>.

**3.3 Powder X-ray diffraction.** The diffraction pattern of the powder sample and of single crystals grinded in agate mortar are shown in fig. 4, panels A and B, respectively. No relevant differences were detected in the positions of the reflections, while the trend of the intensities of the peaks is different. This phenomenon is evidently due to preferred orientation effects present in the grinded single crystals. In order to minimize preferred orientation artifacts the Rietveld refinement procedure was performed on the pattern obtained from the powder sample. The cif file generated from the single crystal data was used for the refinement. The procedure was carried out to attain the unit cell parameters at room temperature (298 K) by taking into account that the single crystal data had been acquired at 100 K. The Le Bail fit (figure S1 of the Supporting Information) is in excellent agreement with the experimental pattern. The peaks that were not fitted correspond to the most intense reflections of  $\text{PbI}_2$ , which is evidently present as impurity. A comparison between the cell parameters achieved at room temperature and at 100 K is reported in table 2. The *b* axis length is more affected by the temperature increase (4% elongation) than the *a* and *c* axes (0.5% for both). Such a result can be justified by the weakness of the interlayer interactions along the *b* axis. This speculation is verified by the easy removal of the solvent intercalated between the layers (see 3.2).

**3.4 TG-DTA/QMS-EGA.** TG-DTA patterns of the powder product after multiple washes with toluene (i.e. to remove as much sulfolane as possible) and with hexane are displayed in fig. 5 panel A. An endothermic event occurred at 80 °C. In order to assess the nature of the event (i.e. either polymorphic transition or melting), another portion of the same sample was heated gently in a beaker and began melting at about 80 °C. This result was quite surprising. Indeed, to the best of authors' knowledge, no ammonium lead halide is reported to melt before decomposing. At 103 °C the material started to decompose. The decomposition occurred in two stages. In fact, two exothermic events, with two distinct weight loss trends, could be detected. This is more evident in the panels B and C of fig. 5, in which the TG and DTA signals are compared with the derivative of the TG, respectively. The exothermic decomposition ends at 227 °C and at 277 °C another weight loss process occurs, but this is an endothermic one. By considering the composition of the sample, the exothermic events can be safely attributed to the decomposition of the hydroxylammonium iodide (hydroxylammonium compounds are well known to decompose exothermally<sup>32,33</sup>), whereas the endothermic event can be

ascribed to the loss of sulfolane. The latter attribution is further supported by the fact that the corresponding weight loss started at 277 °C and the boiling point of sulfolane is 285 °C. Another endothermic event with no weight loss occurred at 410 °C and it corresponds to the melting point of lead iodide. The sulfolane loss accounts for 10.55 wt. %, while the hydroxylammonium iodide loss is 22.75 wt. %. The ratio between the hydroxylammonium iodide content and the total mass minus the sulfolane content is 25.4%, in excellent agreement with the  $\text{NH}_3\text{OHPbI}_3$  composition (25.9% theoretical). During the loss of hydroxylammonium iodide, the composition of the evolved gases transported by the argon purge flow was monitored by means of quadrupole mass spectrometry. The maximum intensity of the ion currents produced by the evolved gases was recorded when the sample temperature was around 150 °C. The difference between the mass spectrum of the bare carrier gas and during the evolution of the gases with maximum ion current intensities is shown in fig. 6. Peaks were found for  $m/z$  values 44, 32, 30, 28 and 14 and were attributed to  $\text{N}_2\text{O}$  (44),  $\text{O}_2$  (32),  $\text{NO}$  (30) and  $\text{N}_2$  (28 and 14).  $\text{N}_2\text{O}$ ,  $\text{NO}$  and  $\text{N}_2$  are the expected gaseous products of the thermal decomposition of hydroxylamine<sup>34</sup> while  $\text{O}_2$  was very probably produced in the ion source by the decomposition of  $\text{N}_2\text{O}$ . Thus, TG-DTA results in conjunction with the QMS analysis of the evolved gases confirm both the presence of hydroxylamine in the sample and the expected stoichiometry of  $\text{NH}_3\text{OHPbI}_3$ .

**3.5 UV-Vis spectroscopy.** The pseudoabsorbance spectrum of the powder product is shown in fig. 7, and the corresponding Tauc's plot in fig. 8. Three absorption maxima are present, the first at 500 nm, the second at 386 nm and the third at 293 nm in order of increasing intensity. The Tauc's plot gives the best agreement to the pseudoabsorbance spectrum for a direct allowed band gap transition corresponding to the cutoff wavelength of the second peak, i.e. 442 nm that in turn corresponds to a band gap of 2.8 eV. Specifically, the band gap energy obtained through the Tauc's plot is  $2.88 \pm 0.01$  eV. Such a value is associated to a Shockley-Queisser energy conversion efficiency limit<sup>35</sup> around 8-9%. These findings, combined with the high chemical reactivity, render  $\text{NH}_3\text{OHPbI}_3$  totally unsuitable for photovoltaic applications.

**3.6 FT-IR spectroscopy.** Because of the relatively high sulfolane content in the samples, a comparison between the spectra of powder sample and sulfolane both dispersed in KBr was mandatory in order to isolate the sulfolane absorptions. Both spectra are displayed in fig. 9. The spectrum of the sample is clearly dominated by sulfolane absorptions, and in the portion extending from 400 to 1400  $\text{cm}^{-1}$  only sulfolane absorptions are visible. Overall, only three absorptions can be ascribed to the hydroxylammonium ion. Needless to say, the vibrations related to the Pb-I part of the structure are out of the explored energy range. The wavenumbers corresponding to these absorptions are 1510, 2700 and 3090  $\text{cm}^{-1}$ . They first can be assigned to deformation mode of  $-\text{NH}_3^+$ , the second

to combination between  $\text{-NH}_3^+$  rocking and deformation modes, and the third to the  $\text{-OH}$  and  $\text{-NH}_2$  stretching vibrations<sup>36</sup>. New Article Online  
DOI: 10.1039/C9DT00690G

**3.7 ESI-MS.** The chemical identity of material was further verified by the positive ions ESI mass spectrum (fig. 10). All the peaks belong to hydroxylamine adducts and decomposition products, with the exception of the one with the highest value of  $m/z$ , which can be attributed to a mono-demethylated fragment of the solvent.

**3.10 CHNS analysis.** The analysis was performed on a sample of single crystals, giving the following wt. % values: C=5.89%, H=1.61%, N=1.65% S=3.59%. The C/S weight ratio is in good agreement with the expected value for sulfolane (calculated: 1.5, found 1.6). By using these values, an estimated sulfolane content of 14 wt. % for the compound was found. Such a result corroborates the 16 wt. % calculated from the crystal structure. The N content is also in good agreement with the  $\text{NH}_3\text{OHPbI}_3$  stoichiometry provided that the sulfolane content is taken into account (calculated: 2.2%, found: 1.9%). Similar considerations apply to the expected H/N weight ratio for  $\text{NH}_3\text{OH}^+$  (calculated: 0.3, found: 0.4).

**3.11  $^1\text{H}$  NMR.** The presence of hydroxylammonium moiety in the compound was once again confirmed by the  $^1\text{H}$ -NMR spectrum collected from a sample of single crystals dissolved in deuterated dimethylsulfoxide. Two broad signals at  $\delta$  9.85 (1H) and  $\delta$  10.05 (3H) were assigned to hydroxyl and ammonium protons, respectively. The chemical shift and the shape of ammonium hydrogen signal are agreement with literature spectral data of organic hydroxylammonium compounds in the same solvent<sup>37</sup>.

## 4. Conclusion

Hydroxylammonium lead iodide  $\text{NH}_3\text{OHPbI}_3$  synthesis could be accomplished only after a careful choice of the solvent and experimental conditions. The conventional approaches used for the syntheses of many other ammonium lead halide perovskites (i.e. Poglitsch method, crystallization from DMF solutions) turned out not to be effective in the case of the hydroxylammonium lead iodide perovskite. On the other hand, the use of sulfolane as solvent for the synthesis allowed to achieve the desired product. XRD single crystal structural analysis showed a layered, low density structure in which the layers, lying on the  $ac$  plane, are comprised of  $\text{NH}_3\text{OH}^+$  chains interposed between chains of face sharing  $\text{PbI}_6$  octahedra. Sulfolane molecules easily intercalate between the layers due to the favorable interactions with hydroxylammonium ions. The existence of weak interlayer interactions was confirmed by powder XRD that demonstrated the high sensitivity of the  $b$  axis length to temperature variation compared to the  $a$  and  $c$  axes. The chemical identity of the compound was checked and verified by different physico-chemical techniques. The compound clearly violates the

Goldschmidt's tolerance factor. Indeed,  $\text{NH}_3\text{OHPbI}_3$  does not possess the expected perovskite structure. Furthermore, its instability, reactivity and inadequate band gap value preclude any possible use in photovoltaic devices.

### **Acknowledgements**

The authors wish to thank the Università degli Studi di Roma "La Sapienza" for financial support and the Elettra-Sincrotrone Trieste S.C.p.A for making available beamtime at the XRD1 beamline.

The authors wish to thank the crystallography Reviewer for his/her truly valuable contribution to the crystal structure refinement.

### **Associated Content**

The CIF (crystallographic information file) of the determined crystal structure is available. Supporting Information file is available.

## References

- <sup>1</sup> A. Cicciooli; A. Latini. Thermodynamics and the Intrinsic Stability of Lead Halide Perovskites  $\text{CH}_3\text{NH}_3\text{PbX}_3$ . *J. Phys. Chem. Lett.* 2018, 9, 3756–3765.
- <sup>2</sup> M Grätzel. The Rise of Highly Efficient and Stable Perovskite Solar Cells. *Acc. Chem. Res.* 2017, 50, 487–491.
- <sup>3</sup> G. Kieslich; S. Sun; A.K. Cheetham. An extended Tolerance Factor approach for organic–inorganic perovskites. *Chem. Sci.* 2015, 6, 3430–3433.
- <sup>4</sup> M, Becker; M. Wark. Organic Cation Substitution in Hybrid Perovskite  $\text{CH}_3\text{NH}_3\text{PbI}_3$  with Hydroxylammonium ( $\text{NH}_3\text{OH}^+$ ): A First-Principles Study. *J. Phys. Chem. C* 2018, 122, 3548–3557.
- <sup>5</sup> E.V. Campbell; B. Dick; A.L. Rheingold; C. Zhang; X. Liu; Z.V. Vardeny; J.S. Miller. Structures of a Complex Hydrazinium Lead Iodide,  $(\text{N}_2\text{H}_5)_{15}\text{Pb}_3\text{I}_{21}$ , Possessing  $[\text{Pb}_2\text{I}_9]^{5-}$   $[\text{PbI}_6]^{4-}$ , and I<sup>-</sup> Ions and  $\alpha$ - and  $\beta$ - $(\text{N}_2\text{H}_5)\text{PbI}_3$ . *Chem. Eur. J.* 2018, 24, 222–229.
- <sup>6</sup> W.P. Jencks; M. Gilchrist. The Reaction of Hydroxylamine with Amides. Kinetic Evidence for the Existence of a Tetrahedral Addition Intermediate. *J. Am. Chem. Soc.* 1964, 86, 5616–5620.
- <sup>7</sup> D. Davidson. Hydroxamic acids in qualitative organic analysis. *J. Chem. Educ.* 1940, 17, 81–84.
- <sup>8</sup> M. Aamira; Z.H. Shahb; M. Shera; A. Iqbalb; N. Revaprasaduc; M.A. Malikd; J. Akhtare. Enhanced photocatalytic activity of water stable hydroxyl ammonium lead halide perovskites. *Mater. Sci. Semicond. Process.* 2017, 63, 6–11.
- <sup>9</sup> A. Poglitsch; D. Weber. Dynamic disorder in methylammoniumtrihalogenoplumbates (II) observed by millimeter-wave spectroscopy. *J. Chem. Phys.* 1987, 87, 6373–6378.
- <sup>10</sup> B. Brunetti; C. Cavallo; A. Cicciooli; G. Gigli; A. Latini. On the Thermal and Thermodynamic (In)Stability of Methylammonium Lead Halide Perovskites. *Sci. Rep.* 2016, 6, 31896.
- <sup>11</sup> A. Latini; G. Gigli; A. Cicciooli. A study on the nature of the thermal decomposition of methylammonium lead iodide perovskite,  $\text{CH}_3\text{NH}_3\text{PbI}_3$ : an attempt to rationalise contradictory experimental results. *Sustainable Energy Fuels* 2017, 1, 1351–1357.
- <sup>12</sup> R. Panetta; G. Righini; M. Colapietro; L. Barba; D. Tedeschi; A. Polimeni; A. Cicciooli; A. Latini. Azetidinium Lead Iodide: Synthesis, Structural and Physico-Chemical Characterization. *J. Mater. Chem. A*, 2018, 6, 10135–10148.
- <sup>13</sup> A. Mancini; P. Quadrelli; G. Amoroso; C. Milanese; M. Boiocchi; A. Sironi; M. Patrini; G. Guizzetti; L. Malavasi. Synthesis, structural and optical characterization of  $\text{APbX}_3$  (A=methylammonium, dimethylammonium, trimethylammonium; X=I, Br, Cl) hybrid organic-inorganic materials. *J. Solid State Chem.* 2016, 240, 55–60.

- <sup>14</sup> N. Ahn; D. Son; I. Jang; S.M. Kang; M. Choi; N. Park. Highly Reproducible Perovskite Solar Cells with Average Efficiency of 18.3% and Best Efficiency of 19.7% Fabricated via Lewis Base Adduct of Lead(II) Iodide. *J. Am. Chem. Soc.* 2015, 137, 8696–8699. New Article Online  
DOI: 10.1039/C9DT000890G
- <sup>15</sup> C. Laurence; J.F. Gal. Lewis Basicity and Affinity Scales Data and Measurement, Wiley, 2010, p. 76.
- <sup>16</sup> F. Cataldo. A revision of the Gutmann donor numbers of a series of phosphoramides including TEPA. *Eur. Chem. Bull.* 2015, 4, 92-97.
- <sup>17</sup> U. Tilstam. Sulfolane: A Versatile Dipolar Aprotic Solvent. *Org. Process Res. Dev.* 2012, 16, 1273-1278.
- <sup>18</sup> B. J. Barker; J. Rosenfarb; J.A. Caruso. Ureas as Solvents for Chemical Investigations. *Angew. Chem. Int. Ed. Engl.* 1979, 18, 503-507.
- <sup>19</sup> A. Lausi; M. Polentarutti; S. Onesti; J.R. Plaisier; E. Busetto; G. Bais; L. Barba; A. Cassetta; G. Campi; D. Lamba; A. Pifferi; S.C. Mande; D.D. Sarma; S.M. Sharma; G. Paolucci. Status of the crystallography beamlines at Elettra. *Eur. Phys. J. Plus* 2015, 130, 43.
- <sup>20</sup> S. Bernstorff; E. Busetto; C. Gramaccioni; A. Lausi; L. Olivi; F. Zanini; A. Savoia; M. Colapietro; G. Portalone; M. Camalli; A. Pifferi; R. Spagna; L. Barba; A. Cassetta. The macromolecular crystallography beamline at ELETTRA. *Rev. Sci. Instrum.* 1995, 66, 1661-1664.
- <sup>21</sup> W. Kabsch. XDS. *Acta Cryst.* 2010, D66, 125-132.
- <sup>22</sup> L. Palatinus; G. Chapuis. SUPERFLIP - a computer program for the solution of crystal structures by charge flipping in arbitrary dimensions. *J. Appl. Cryst.* 2007, 40, 786-790.
- <sup>23</sup> O.V. Dolomanov; L.J. Bourhis; R.J. Gildea; J.A.K. Howard; H. Puschmann. Olex2: A complete structure solution, refinement and analysis program. *J. Appl. Cryst.* 2009, 42, 339-341.
- <sup>24</sup> G.M. Sheldrick. Crystal structure refinement with ShelXL, *Acta Cryst.* 2015, C71, 3-8.
- <sup>25</sup> A.L. Spek. Structure validation in chemical crystallography. *Acta Cryst.* 2009, D65, 148-155.
- <sup>26</sup> L. Lutterotti; D. Chateigner; S. Ferrari; J. Ricote. Texture, Residual Stress and Structural Analysis of Thin Films using a Combined X-Ray Analysis. *Thin Solid Films* 2004, 450, 34-41.
- <sup>27</sup> J. Tauc; R. Grigorovici; A. Vancu. Optical properties and electronic structure of amorphous germanium. *Phys. Status Solidi* 1966, 15, 627-637.
- <sup>28</sup> T. Kumar; M. Ramya; V. Srinivasan; N. Xavier. A Simple and Direct LC–MS Method for Determination of Genotoxic Impurity Hydroxylamine in Pharmaceutical compounds. *J. Chromatogr. Sci.* 2017, 1-7.
- <sup>29</sup> T. C. Bissot; R.W. Parry; D.H. Campbell. The Physical and Chemical Properties of the Methylhydroxylamines. *J. Am. Chem. Soc.* 1957, 79, 796-800.

- <sup>30</sup> D. Vinci; M. Donaldson; J.P. Hallett; E.A. John; P. Pollet; C.A. Thomas; J.D. Grilly; P.G. Jessop; C.L. Liotta; C.A. Eckert. Piperylene sulfone: a labile and recyclable DMSO substitute. *Chem. Commun.* 2007, 1427-1429. View Article Online  
DOI: 10.1039/C9DT000890G
- <sup>31</sup> L. Meng; Z. Lu; Y. Ma; X. Xue; F. Nie; C. Zhang. Enhanced Intermolecular Hydrogen Bonds Facilitating the Highly Dense Packing of Energetic Hydroxylammonium Salts. *Cryst. Growth Des.* 2016, 16, 7231-7239.
- <sup>32</sup> T. Grewer. The influence of Chemical structure on exothermic decomposition. *Thermochim. Acta* 1991, 187, 133-149.
- <sup>33</sup> L.O. Cisneros; W.J. Rogers; M.S. Mannan. Comparison of the thermal decomposition behavior for members of the hydroxylamine family. *Thermochim. Acta* 2004, 414, 177-183.
- <sup>34</sup> L.O. Cisneros; X. Wu; W.J. Rogers; M.S. Mannan; J. Park; S.W. North. Decomposition products of 50% mass hydroxylamine/water under runaway reaction conditions. *Process Saf. Environ.* 2003, 81, 121-124.
- <sup>35</sup> W. Shockley; H. J. Queisser. Detailed Balance Limit of Efficiency of p-n Junction Solar Cells. *J. Appl. Phys.* 1961, 32, 510-519.
- <sup>36</sup> D.L. Frasco; E.L. Wagner. Interpretation of the Infrared Spectra of the Solid Hydroxylammonium Halides. *J. Chem. Phys.* 1959, 30, 1124-1130.
- <sup>37</sup> N. Fischer; T.M. Klapötke; D.G. Piercey; J. Stierstorfer. Hydroxylammonium 5-Nitriminotetrazolates. *Z. Anorg. Allg. Chem.* 2012, 638, 302-310.

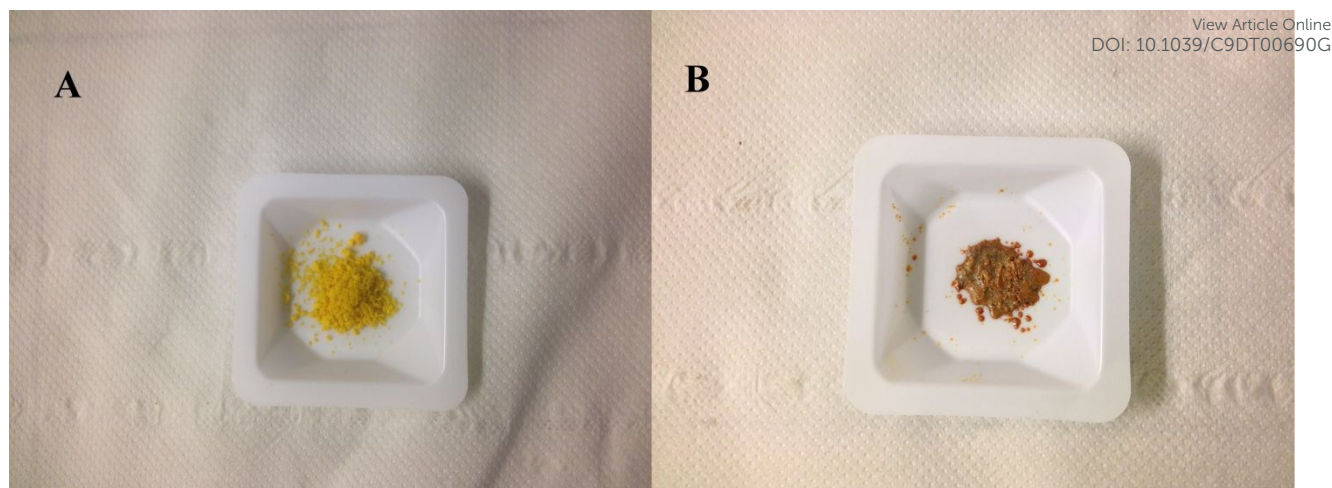


Fig. 1. Panel A:  $\text{NH}_3\text{OHPbI}_3$  powder freshly prepared by sulfolane extraction with toluene. Panel B: the same sample after 3 days under ambient conditions.

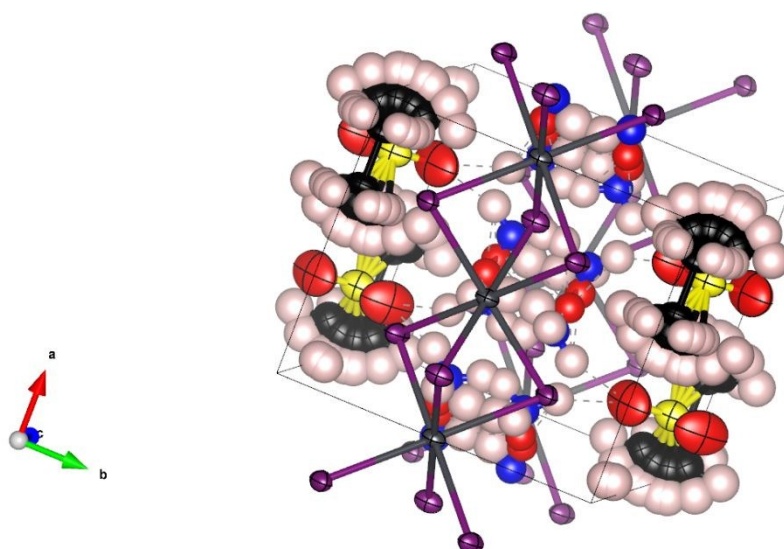


Fig. 2. Representation of the unit cell of  $\text{NH}_3\text{OHPbI}_3$  with sulfonate molecules layers between the Pb-I- $\text{NH}_3\text{OH}$  layers. Red ellipsoids: oxygen atoms; yellow ellipsoids: sulfur atoms; black ellipsoids: carbon atoms; creamy-white ellipsoids: hydrogen atoms; blue ellipsoids: nitrogen atoms; dark grey ellipsoids: lead atoms; purple ellipsoids: iodine atoms. The probability used to depict the thermal ellipsoids is 50%. Apparent multiple positions of each carbon and hydrogen atom of sulfonate molecules are due to the modeling of their disorder.

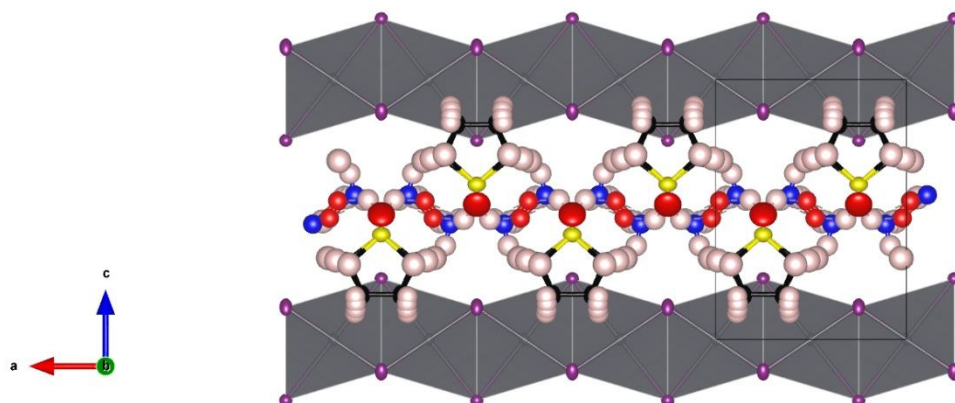


Fig. 3. The crystal structure of  $\text{NH}_3\text{OHPbI}_3$  seen along the  $b$  axis. The sinusoidal arrangement of  $\text{NH}_3\text{OH}^+$  ions along the  $a$  direction is clearly visible.

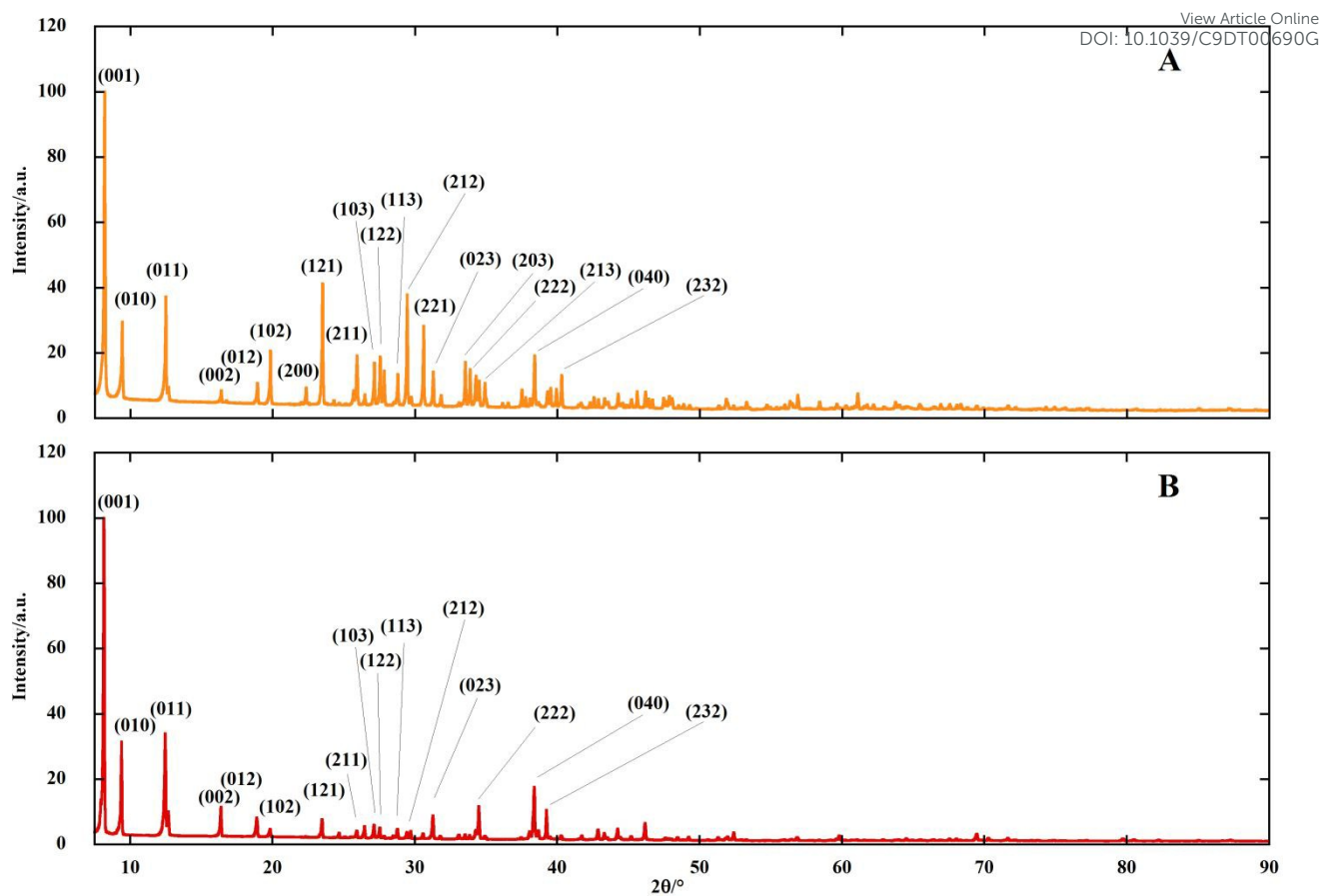


Fig. 4. Panel A: powder diffraction pattern of  $\text{NH}_3\text{OHPbI}_3$  powder prepared by sulfolane extraction with toluene. Panel B: powder diffraction pattern of  $\text{NH}_3\text{OHPbI}_3$  single crystals grinded in agate mortar. The assignment of the most important reflections is reported.

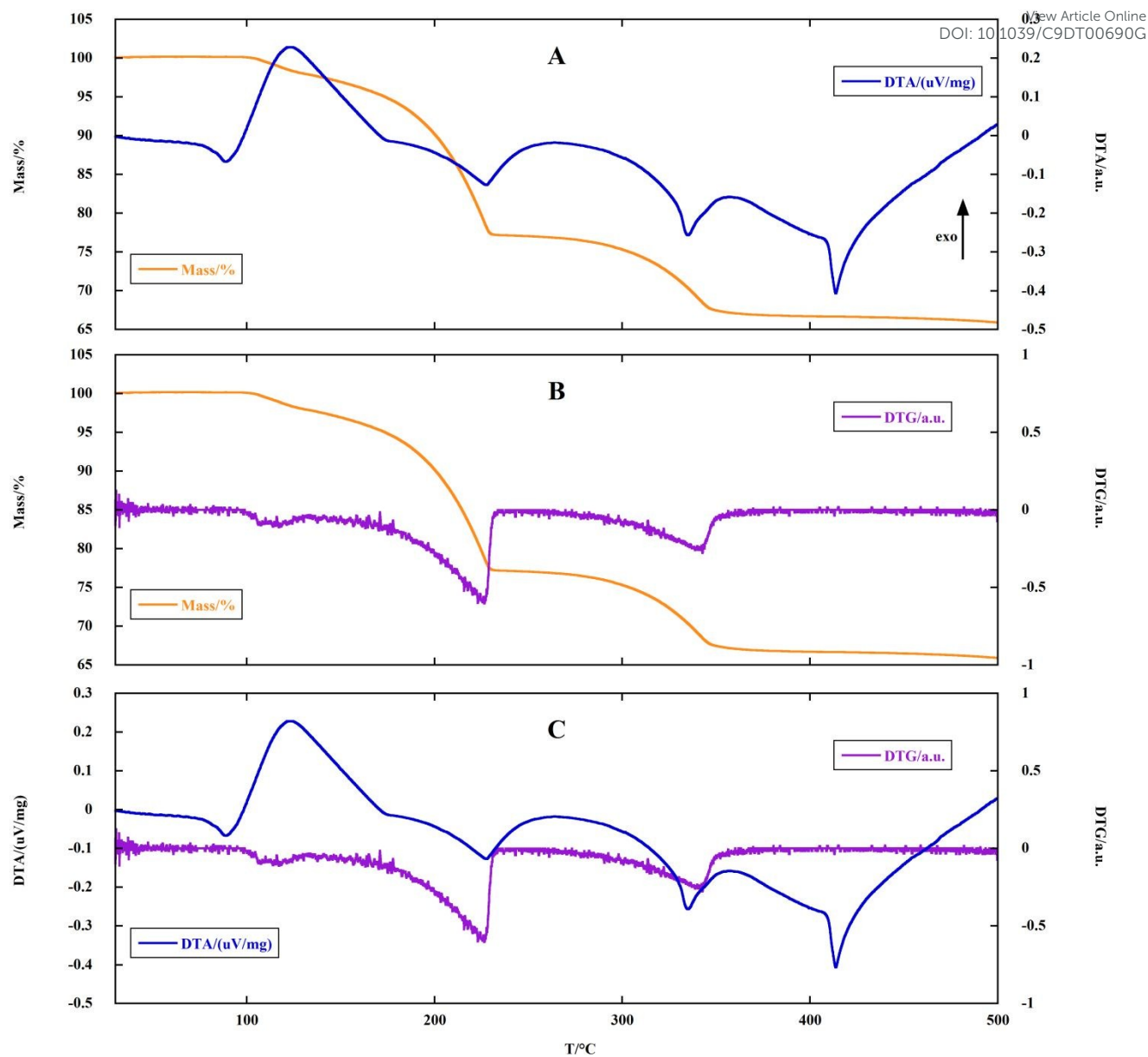


Fig. 5. Panel A: TG and DTA profiles of  $\text{NH}_3\text{OHPbI}_3$  powder prepared by sulfolane extraction with toluene and washed multiple times with toluene. Panel B: TG profile and its derivative. Panel C: DTA profile and the derivative of TG profile.

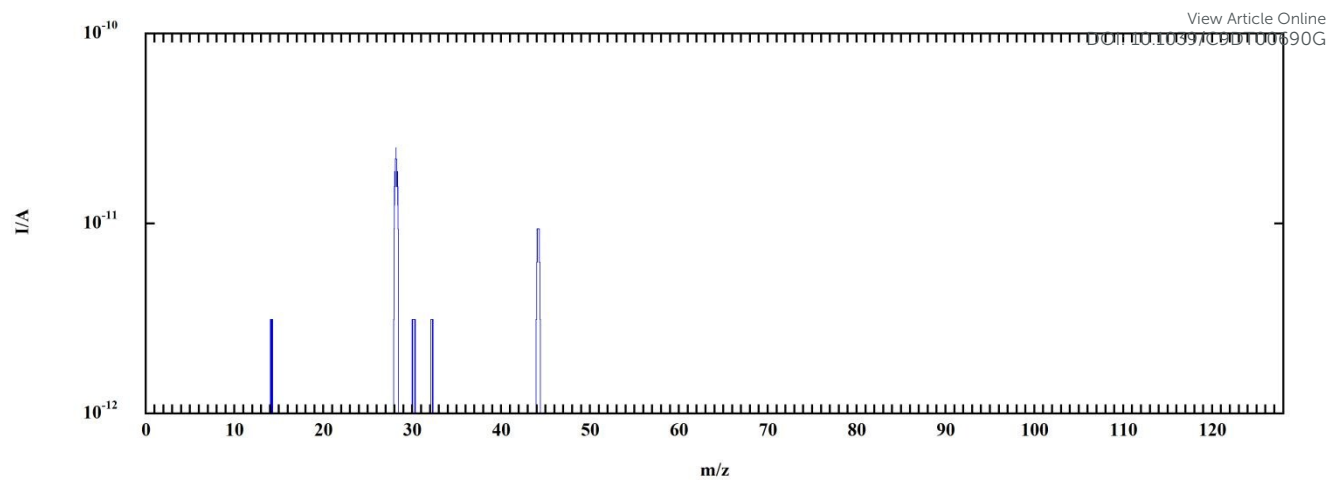


Fig. 6. Difference between the mass spectrum of the carrier gas (argon) used in the TG-DTA measurement before and during the maximum gas evolution from the sample. Peaks are visible for  $m/z$  values 44, 32, 30, 28 and 14.

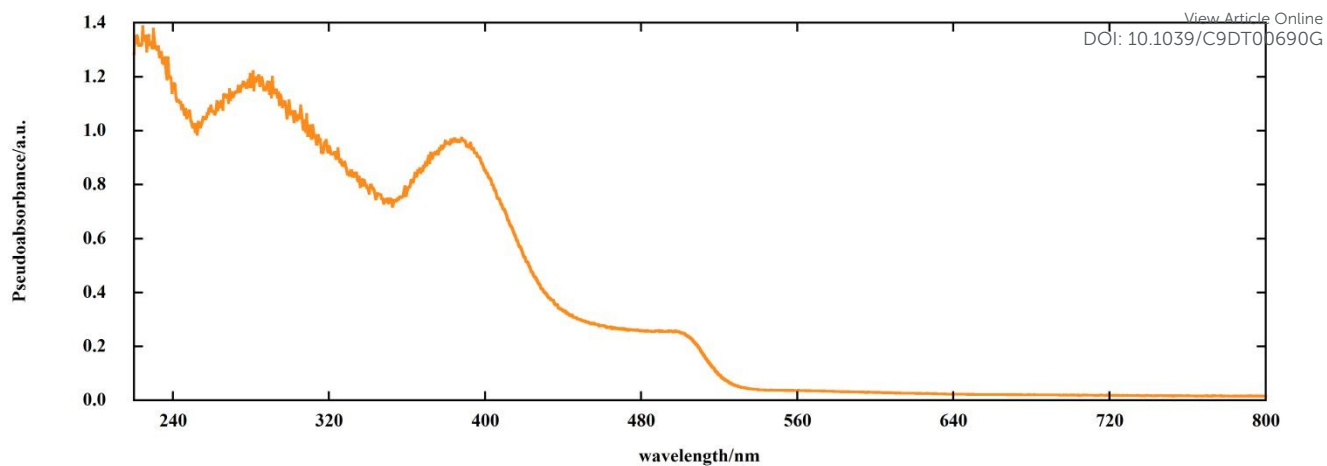


Fig. 7. Diffuse reflectance UV-Vis spectrum of  $\text{NH}_3\text{OHPbI}_3$  powder.

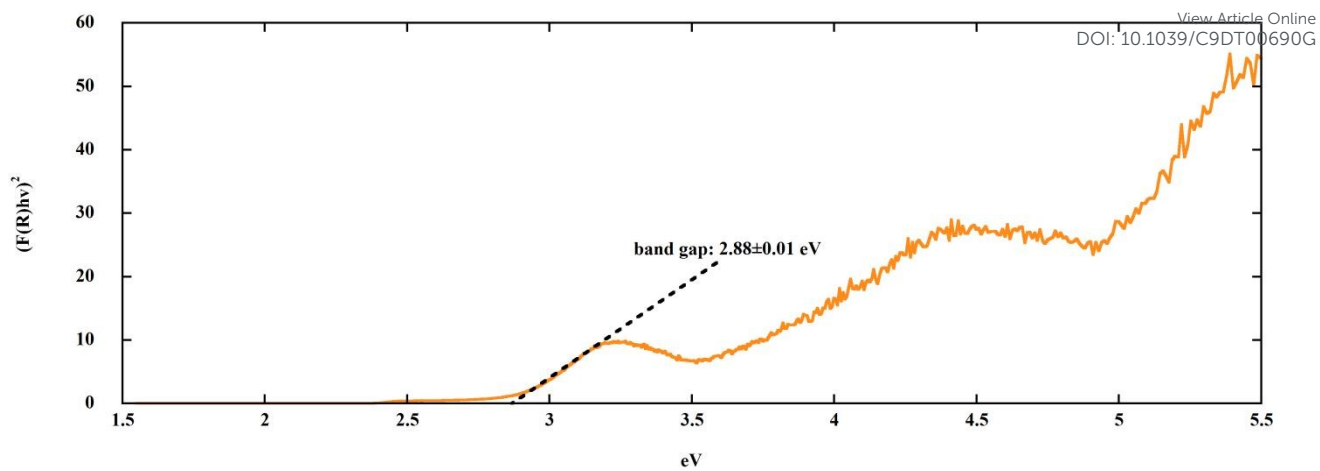


Fig. 8. Tauc's plot of the UV-Vis reflectance spectrum assuming an allowed direct band gap transition.

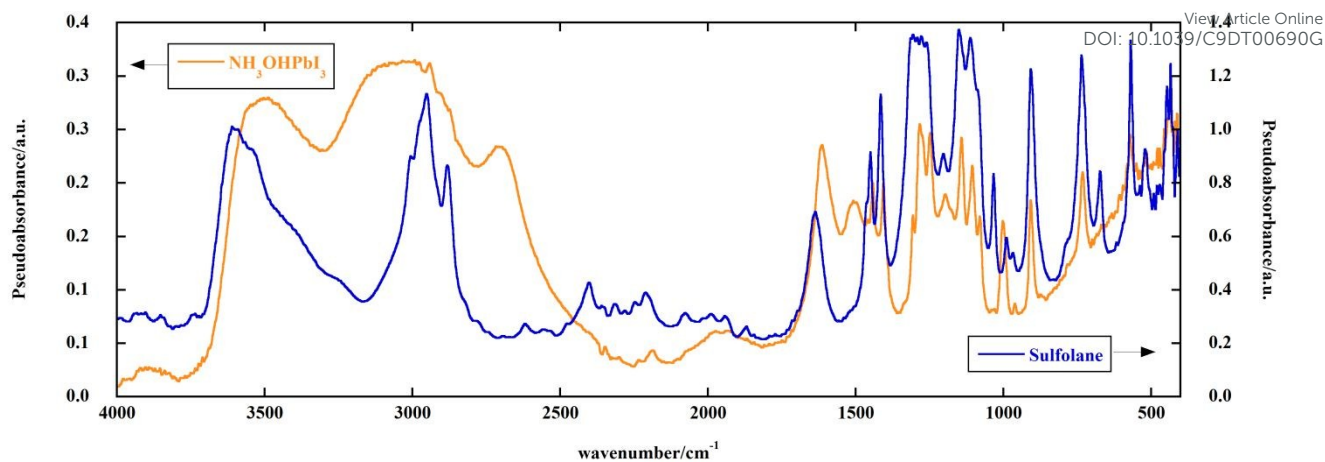


Fig. 9. FT-IR diffuse reflectance spectra of  $\text{NH}_3\text{OHPbI}_3$  powder (yellow orange line) and sulfolane (blue line) both dispersed in KBr.

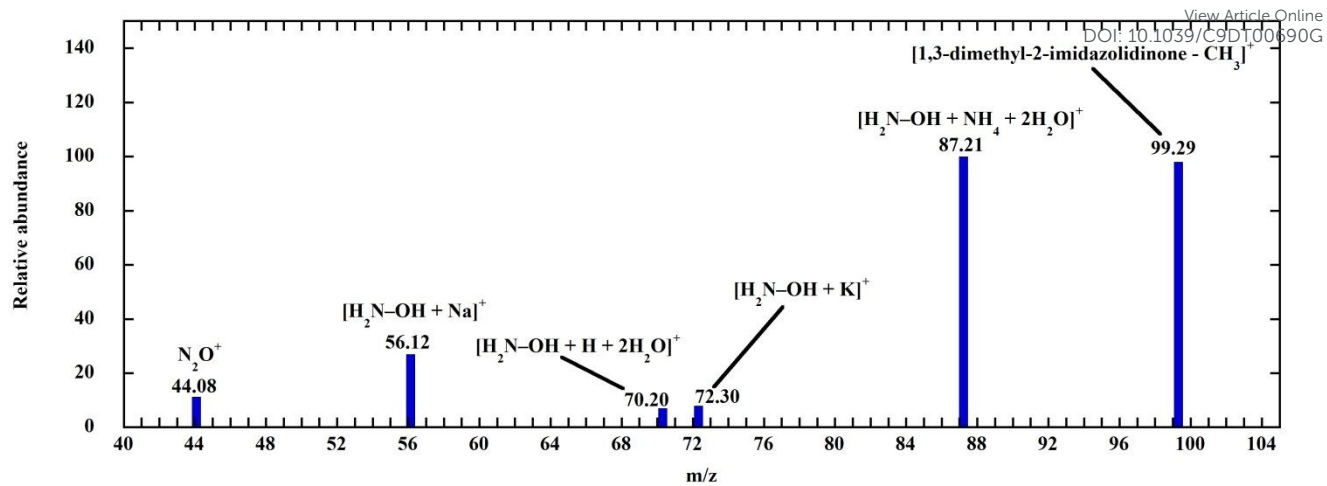


Fig. 10. ESI-MS spectrum (positive ions) of  $NH_3OHPbI_3$  dissolved in DMI.

Formula	C <sub>6</sub> H <sub>20</sub> I <sub>3</sub> NO <sub>3</sub> PbS
$D_{calc.}/\text{g cm}^{-3}$	3.338
$\mu/\text{mm}^{-1}$	17.091
Formula Weight	774.18
Colour	light yellow
Shape	polyhedral
Size/mm <sup>3</sup>	0.07×0.05×0.05
$T/\text{K}$	100
Crystal System	orthorhombic
Space Group	<i>Pmma</i>
$a/\text{Å}$	7.920(6)
$b/\text{Å}$	9.030(4)
$c/\text{Å}$	10.770(2)
$\alpha/^\circ$	90
$\beta/^\circ$	90
$\gamma/^\circ$	90
$V/\text{Å}^3$	770.25(1)
$Z$	2
$Z'$	0.25
Wavelength/Å	0.700
Radiation type	Synchrotron
$\vartheta_{min}/^\circ$	2.221
$\vartheta_{max}/^\circ$	30.974
Measured Refl.	6502
Independent Refl.	1360
Reflections with $I > 2\sigma(I)$	1271
$R_{int}$	0.0392
Parameters	56
Restraints	20
Largest Peak	1.860
Deepest Hole	-2.248
GooF	1.151
$wR_2$ (all data)	0.1259
$wR_2$	0.1239
$R_1$ (all data)	0.0413
$R_1$	0.0394

Table 1. Crystallographic data of NH<sub>3</sub>OHPbI<sub>3</sub>.

Cell parameters (Å)	Single crystal (100 K)	Powder (298 K)
<i>a</i>	7.920(6)	7.9624(5)
<i>b</i>	9.030(4)	9.3919(6)
<i>c</i>	10.770(2)	10.8248(8)

View Article Online  
DOI: 10.1039/C9DT00690G

Table 2. Comparison of unit cell parameters obtained at 100 K (single crystal data) and at 298 K (powder data).